Lawrence Berkeley National Laboratory
Recent Work

Title

A SCINTILLATION COUNTER ARRAY FOR DETECTION OF HIGH ENERGY NEUTRONS

Permalink

https://escholarship.org/uc/item/3wd5z8dw

Authors

Parsons, Anthony S. L.
Truoel, Peter
Berardo, Peter A.
et al.

Publication Date

1969-07-01

A SCINTILLATION COUNTER ARRAY FOR DETECTION OF HIGH ENERGY NEUTRONS

Anthony S. L. Parsons and Peter Truoel
and
Peter A. Berardo, Roy P. Haddock, Lynn Verhey, and
Michael E. Zeller

July 1969

LAWRENCE RADIATION LABORATORY
UNIVERSITY of CALIFORNIA BERKELEY

UCRL-19259

DISCLAIMER

A SCINTILLATION COUNTER ARRAY FOR DETECTION
OF HIGH ENERGY NEUTRONS

Anthony S. L. Parsons[*] and Peter Truoel[†]

Lawrence Radiation Laboratory
University of California
Berkeley, California 94720

and

Peter A. Berardo, Roy P. Haddock, Lynn Verhey, and
Michael E. Zeller[††]

University of California at Los Angeles, California

August 1969

ABSTRACT

An array of 32 liquid scintillation counters used to detect neutrons
in the energy range 20 to 340 MeV is described. Each unit consisted of
a cylinder 45 cm long and 7 cm in diameter, with the axis of the cylinder
parallel to the incident neutron direction. The array was calibrated in
the above energy range by use of neutron-proton elastic scattering. The
average efficiency was 0.45. Some secondary properties of the array
have been studied and are described.

[*] Now at Rutherford High Energy Laboratory, Berkshire, England

[†] On leave from Schweizerisches Institut für Nuklearforschung, Zürich

[††] Present address: Department of Physics, Yale University, New Haven, Conn.

Introduction

In order to measure differential cross sections for the process $\pi^- p \to n\gamma$ we have constructed and calibrated an array of neutron detectors. The requirements of this experiment dictated the following design and operational criteria for the neutron counters:

1. High detection efficiency for neutrons ranging in energy from 20 to 340 MeV.

2. Good spatial resolution per counter, with a total array size which would match the solid angle of the spark chamber which detected the photon.

3. Well-determined detection efficiency over the necessary neutron energy region.

The construction and calibration of similar detectors has been described by several authors[1-5]; however, the demands of good spatial resolution, high efficiency, and accurate efficiency determination were not so great in their work as in this application.

The method of calibration used was neutron-proton elastic scattering. Detection of the recoil proton tags the presence of a neutron in a well-defined direction, and a counter placed in this "beam" of neutrons may be calibrated. This method of tagging has been previously used by other authors[6].

Design and Construction

To make the angular resolution of the neutron compatible with other contributions to the resolution, a 20-mr definition was required. Considerations of the solid angle, time-of-flight path, and matching of array size to the photon spark-chamber solid angle led to the choice

of a neutron detector consisting of a 7-cm-diameter cylinder, 45 cm

long, placed 365 cm from the target. The detection array contained 32

such cylinders mounted 9 cm apart (center to center), as shown in fig. 1.

This spacing was chosen after preliminary measurements on the proba-

bilities of scattering of incident neutrons from one counter into another.

The scintillating material chosen was a liquid, NE 224[7]. The

base for the liquid was pseudo-cumene, which has the advantage over

other possible solvents that it does not interact significantly with Lucite

and other materials. Liquid scintillator is superior to most solids, as

it has a higher hydrogen content and lower light-absorption coefficient in

the spectral region of the scintillations. The major drawback of liquids

is their large dependence of volume on temperature. This required

installation of vent lines on each counter to permit expansion of the

liquid without breaking the container. Air-conditioning the region

around the neutron-counter array minimized the effects of temperature

fluctuations during the experiments.

The basis for the construction was a Lucite tube of 7.6 cm outside

diameter with a 0.32-cm wall. Details are shown in fig. 2. Before the

design was completed, tests were made on prototype counters. The type

of reflective surface placed around the tube was studied as a function of

"absorption length" along the tube for scintillations from a ^{60}Co source.

A spectral reflecting surface was chosen. The stability of the response

of the liquid scintillator when it was in contact with various components

of the counter--i.e. Lucite, Lucite cement, air, etc. --was also studied.

For the materials used in the counters, no significant loss in response

was observed during several months of testing.

The photomultiplier tube used was an RCA 8575. This tube was chosen because of its high quantum efficiency (approximately 28%), high gain (approximately 10^8), and low dark current (approximately 10^{-9} A).

An important factor in the design of the system was the type of discriminator to be used with the phototube. We chose an EGG type 140 discriminator[8] which has the following property: the presence of an output pulse is determined when the leading edge of the pulse exceeds a given pulse height (as in a conventional discriminator); the timing of the output pulse is determined when the input pulse, appropriately clipped, crosses zero. The single unit has the properties of a system that would normally require two discriminators and an "AND" circuit. The EGG 140 is "fixed level", and the bias on a given counter was adjusted by varying the high voltage on the phototube. The dynode signals were used to give pulse-height information.

The biases on the 32 counters were set to be equal in the following manner. With a ^{60}Co source placed at a standard geometrical position on a counter, two pulse-height distributions were obtained: one gated by the anode discriminator, and one ungated. The high voltage on the tube was then adjusted until the lower limit of the gated spectrum corresponded to the upper limit of the ungated ^{60}Co distribution (see fig. 3). The lower limit is determined by the discrimination level on the anode signal; the upper limit represents the Compton scattering end point of ^{60}Co. Each tube is thereby set at an electron bias level of about 1.3 MeV. The reproducibility of this method in terms of the efficiency of the counters for neutron detection was checked extensively at 112 MeV neutron kinetic energy and to a lesser extent at 50 and 20 MeV. Comparison of the

efficiencies of ten counters as well as the efficiency of one counter on
several different occasions is shown in fig. 4.   This method allowed the
bias, in terms of the threshold for a given energy deposited in the scin-
tillator, to be set at the same level for each counter regardless of the
gain of the phototube or the discriminator threshold.

Calibration

        The array was calibrated by use of neutron-proton elastic scat-
tering.   The setup is shown in fig. 5.

        The neutron beam was obtained from the Berkeley 184-inch
cyclotron.   Apart from one calibration measurement at 340 MeV neutron
kinetic energy, the beam was obtained by stripping 450-MeV deuterons
on an internal beryllium target.   This yielded a beam of 204-MeV neu-
trons with full width at half height of 60 MeV.   After collimation, the
beam at the liquid hydrogen target was 3.2 cm high and 2.5 cm wide.
A Polaroid film exposed just downstream from a CH converter in the
beam line determined these dimensions.   For the 340-MeV measurements
the neutrons were produced by 730-MeV protons on beryllium.   The spec-
trum in this case had a peak at 650 MeV, a full width at half height of
about 100 MeV, and a long low-energy tail.   For this energy, collima-
tion was less effective, and the limits of the beam at the target were
consequently less well defined.

        The hydrogen target, a 10.15-cm-diameter vertical cylinder 20
cm high, was the same as used in the main experiment.   To
allow a variable target thickness, the target cylinder was divided by a
0.02-cm-thick vertical Mylar wall perpendicular to the beam.   For the
calibration experiment both halves were filled.   The vacuum jacket was

made of 0.12-cm aluminum with 0.07-cm Mylar entrance and exit windows.
The recoil scattered protons were detected in a differential-range tele-
scope. This telescope consisted of a 2.5×2.5-cm counter placed 14.3 cm
from the target, counters in front of and behind the range at about 200 cm
radius, and an anti-counter behind the differential range. The counter
close to the target (P1) and the well-collimated incident neutron beam
defined an interaction volume in the target which excluded the flask wall[5].
This definition reduced the background due to events not associated with
hydrogen to about 1%.

The direction of the proton in a given event was determined by the
counter P1 and an 8×8 array of 1.27-cm crossed hodoscope counters
placed in front of the differential range counters at a radius of 196 cm
from the target center. The neutron counter array was placed 365 cm
from the target, the same radius as for the main experiment. The counter
P1 also provided a start signal for measurement of the neutron time of
flight.

At 205 MeV incident energy, runs were taken at eight angles cor-
responding to scattered-neutron energies between 20 and 140 MeV. The
upper limit was set by the low energy of the recoil proton. At 650 MeV
incident energy the only practical neutron energy was around 340 MeV.
This energy yielded a maximum in the event rate, since the range in the proton
telescope was not too great, and the solid-angle transformation factors
were still favorable. At each angle the amount of copper range in the
proton telescope was set to give the largest stopping-proton rate in the
differential range. The shape of the range curves obtained reflected the
incident neutron spectrum. The differential range was 2.9 g/cm^2 of copper.

A PDP5 computer was used to monitor the apparatus and to provide a buffer for data storage on magnetic tape. Upon an event trigger, normally a stopping proton, the addresses of the hodoscope and neutron counters that fired and the neutron time of flight and pulse height were recorded and monitored for system stability.

At each angle more than 5×10^4 protons were stopped, yielding about 10^4 events in which a neutron also was detected.

Measurements with empty target were also taken; they showed a contribution of 1 to 2% to the event rate with target full. Random neutrons were less than 1% of the events, and were monitored by use of the time-of-flight information.

The calibration experiment was used to measure the efficiency of the array and to check the spatial- and time-resolution function for reconstruction of the two-body kinematics in the radiative-capture experiment. The background-free sample of two-body events from the neutron-proton scattering data was well suited for this check.

Efficiency Calculation

The measurement of the efficiency was closely coupled to a Monte Carlo simulation of the experiment. This program to generate events included the following effects:

(a) A uniform spatial distribution of neutrons in the beam over the area measured.

(b) The measured energy distribution of neutrons.

(c) Multiple scattering of protons in the target, vacuum jacket, and counters.

(d) Energy selection of protons due to the differential range.

(e) Interaction of neutrons in the target and vacuum jacket.

(f) Computation of the geometrical potential path length (PPL)
of the neutron in a neutron counter, expressed as the fraction
of active counter a given neutron can traverse if it does not
interact.

(g) Neutral cross-scattering in the neutron counter array; in
this process a neutron enters one counter and scatters into
another without the recoil's being detected, but a signal
is produced in the second counter. This effect was measured
in a secondary experiment to be described.

Besides the obvious geometrical effects, (c) and (g) were the main
contributions to the resolution function.

Since the length of a counter was much larger than its radius,
the PPL had a nonnegligible probability of being less than one. The
average PPL determined from the Monte Carlo program was used to
linearly normalize all efficiencies to a full counter length of 45 cm. The
final efficiency is thus the ratio of the experimental to the normalized
geometrical efficiency. This efficiency is shown in fig. 6 and table 1 as
a function of neutron kinetic energy. The calculated efficiency[9] for a
single counter of the appropriate size is shown in fig. 6. The efficiency
of our total array is expectedly higher, since we detect many of the out-
scattered neutrons elsewhere in the array.

Event Reconstruction and Monte Carlo Check

Since the efficiency is strongly dependent on the Monte Carlo
calculation of the mean PPL, it is important to check that the program
correctly simulates the data. Such a check is made with an event-by-
event fitting program. Both the Monte Carlo-generated events and the
data were subjected to the same analysis routine. This routine used the

measured quantities for each event, including the beam direction, mean beam momentum, angles of scattered neutron and proton, and neutron time of flight to compute an overall χ^2 for the event to fit the elastic scattering process. The errors used in computing this χ^2 were geometrical only, i. e. , neutron and proton scattering were not included. The extent to which events lie anomalously far from a χ^2 of zero therefore reflects the amount of such scatterings. The comparison of χ^2 distribution for the data and the Monte Carlo calculation is shown in fig. 7a-c for three energies.

A second check on the Monte Carlo program was made by analyzing data taken with the array at a 198-cm radius. The geometrical effects of this decreased distance are quite large, but since the Monte Carlo program effectively removes the geometrical dependence from the efficiency per PPL, a comparison of the efficiencies measured at the two radii is a check on the Monte Carlo calculation. Figure 7d compares the χ^2 distribution for the data and Monte Carlo for 60-MeV neutron energy with the array at 198 cm.

Neutral and Charged Cross Scattering

Neutral cross-scattering is defined as the detection of a neutron in a counter other than that which it entered; charged cross-scattering is a similar effect except that the recoil is also detected in the first counter. Both processes have the effect of broadening the spatial resolution function. In practice the charged scattering is less serious, since the counter which the neutron first entered can be found by choosing the counter that gives the best fit to the two-body kinematics hypothesis.

Some properties of the charged cross-scattering are summarized in figs. 8 and 9. Figure 8 shows the frequency of charged cross-scattering or multiple events versus the kinetic energy of the neutron.

Figure 9 shows the spatial and time difference between two counters

participating in a double-counter event for two energies. The sharply

peaked time-difference distribution indicates that there is only a small

contribution to the doubles from random neutrons. The spatial distribution

shows that large spatial displacements are not uncommon, and presumably

correspond to a neutron's traversing several counters before reconverting.

The peak at small distances contains the contributions from the charged

recoil particles reaching adjacent counters.

To study neutral cross-scattering the neutron counter array was

placed at 198 cm from the target, thus increasing the rate at which neu-

trons entered the central counters. For each energy two runs of about

10^5 events were recorded, one with the complete array, the second with

one of the central counters removed. The loss of events in all the counters

due to the removal of one counter, corrected for charged cross-scattering

from that counter, was taken as a measure of the neutral cross scattering.

Distributions were measured at three energies, and are presented in

fig. 10. The assumption is made that these distributions measured at

198 cm radius can be used to describe cross-scattering at 365 cm. It is

unlikely that the radius of the array is of primary importance for this

process. The probability of neutral cross-scattering versus energy is

shown in fig. 11.

Application

The efficiency quoted is the efficiency for detection of the neutron

anywhere within the array, not necessarily within the counter initially

entered. This efficiency can be carried over to the main experiment,

as long as a suitable resolution function is used and some correction

factors are applied. These corrections, arising from the lack of exact correspondence between the two experimental arrangements, will now be described.

The most significant correction arose from the difference in the distribution of neutrons entering the array. In the radiative-capture experiment the distribution was essentially uniform; in the calibration experiment the selection of events by the proton telescope produced a distribution which was peaked at the center of the array, and fell almost to zero at the perimeter, simulating an infinite array of counters. Since the efficiency is defined for detection of a neutron anywhere within the array and because the neutral cross-scattering is 10 to 20%, a correction factor must be applied for the relative losses of neutrons out of the side of the array; this loss in each case was computed from the measured neutral cross-scattering distribution. The relative correction was between 2 and 5% with an error of 1%.

The distribution of events in the hydrogen target and consequently the absorption of neutrons leaving the target were different for the calibration and photoproduction experiments. This difference in distributions was due to the different beam profiles, the geometric selection of events by the proton telescope, and (usually) use of only the downstream half of the target in the main experiment whereas the target was full during calibration. The interaction of neutrons was included in Monte Carlo calculations describing both experiments, and allowed a relative correction to be made (less than 1%).

Summary

The method of construction and operation of the neutron counters has proved reliable and repeatable in terms of counter efficiency and

time resolution. The calibration experiment has shown that the neutron-counter array fulfilled the requirements of the experiment for which it was designed. Also, the successful application of the above-mentioned corrections demonstrated the possibility of using the same counters in other configurations.

Acknowledgments

We are grateful to Mr. Ray Belisle, Mr. Carl Brazell, and Mr. Reginald Roberts for valuable technical assistance and to Mr. Norman Gunther for much of the computer programming effort. We also wish to acknowledge the support of Mr. James Vale and the crews of the 184-inch cyclotron, and the LRL and UCLA computing facilities.

References

1. C. E. Wiegand, Tom Elioff, William B. Johnson, Leonard B. Auerbach, Joseph Lach, and Thomas Ypsilantis, Rev. Sci. Instr. 33 (1962) 526.

2. P. H. Bowen, G. C. Cox, G. B. Huxtable, A. Langsford, J. P. Scanlon, G. H. Stafford and J. J. Thrasher, Nucl. Instr. and Meth. 17 (1962) 117.

3. J. B. Czirr and D. R. Nygren, Nucl. Instr. and Meth. 31 (1964) 226.

4. D. E. Crabb, J. G. McEwen, E. G. Auld, and A. Langsford, Nucl. Instr. and Meth. 48 (1967) 87.

5. F. P. Brady, J. A. Jungermann, J. C. Young, J. L. Ronero, and P. J. Symonds, Nucl. Instr. and Meth. 58 (1968) 57.

6. C. E. Wiegand, et al. loc. cit.; F. P. Brady, et al., loc. cit.

7. Obtained from Nuclear Enterprises, Ltd. Winnepeg, Manitoba, Canada.

8. Obtained from EG & G Inc., 35 Congress St., Salem, Mass.

9. Calculation made with computer program by R. J. Kurz, Lawrence Radiation Laboratory Report UCRL-11339, March 1964.

Table I. Detector efficiency as a function of neutron kinetic energy.

T_i^a [MeV]	T_n^b [MeV]	R_n^c [cm]	θ_n [deg]	θ_p [deg]	Range [g/cm²]	Diff. range [g/cm²]	No. of protons stopped (Exp.)	No. of n-p coincidences	Empty target corrections	Random events corrections	No. of protons stopped (M. Carlo)	No. of n-p coincidences	No. of neutron counter lengths traversed	Efficiency per counter length
203	20	365	70.0	18.1	26.0	2.9	49,668	9,163	0.70%d	0.8%	3,359	1,411	1220.0	50.1 ± 1.2
203	30	365	65.8	22.0	23.4	2.9	49,817	11,010	0.70%d	0.7%	2,630	1,277	1121.0	51.8 ± 1.2
203	40	365	61.6	26.0	21.1	2.9	95,594	21,900	0.72%	0.6%	4,010	2,070	1777.1	51.6 ± 1.1
203	52	365	58.0	29.4	17.18	2.9	11,327	2,587	0.75%	0.6%	3,642	1,912	1647.5	50.5 ± 1.4
203	60	365	55.3	32.0	15.8	2.9	140,909	32,961	0.70%	0.6%	3,217	1,761	1528.1	50.7 ± 1.1
203	74	365	51.2	36.0	11.4	2.9	99,661	22,898	0.78%	0.6%	2,390	1,313	1142.6	48.0 ± 1.2
203	112	365	40.0	45.9	4.43	2.9	82,261	17,042	0.58%	0.4%	1,496	778	668.3	46.3 ± 1.6
203	140	365	31.3	56.0	0.0	0.0	50,103	10,258	2.10%	0.8%	1,931	1,091	932.2	42.6 ± 1.2
650	340	365	36.05	45.0	57.9	5.8	2,182	405	0.70%d	0.6%	660	363	325.7	37.6 ± 2.4
203	30	183	67.4	22.0	23.4	2.9	37,192	10,150	1.30%	0.5%	1,030	778	512.5	55.0 ± 2.6
203	60	183	56.9	32.0	15.8	2.9	282,620	75,031	1.30%e	0.4%	7,756	5,707	3810.2	54.3 ± 0.9
203	112	183	41.4	45.9	4.43	2.9	314,700	76,856	1.10%e	0.4%	2,500	1,904	1247.9	49.3 ± 1.5

a) Incident neutron energy.

b) Energy of the scattered neutron.

c) Radius of neutron counter array.

d) Extrapolated.

e) Scaled from 365-cm run.

Figure Legends

Fig. 1. The neutron counter array. (left) Neutron view. The letters
assign counters to one of four independent time-of-flight mea-
suring systems. [For much of the data taking A, B and C.D
were combined to form two systems only.]   (b) Plan view. The
counters focus on a target at 366 cm from the front face.

Fig. 2. Details of the construction of one neutron counter.

Fig. 3. Pulse-height spectra used in setting phototube bias.

Fig. 4. Comparison of the efficiency at 112 MeV (a) for several
counters, (b) for one counter on different occasions.

Fig. 5. Neutron proton elastic scattering setup. The neutron counter
array is offset to allow it to be placed as close as possible to the
π^- beam in the radiative capture experiment.

Fig. 6. Detection efficiency of neutron counter array versus neutron kinetic energy.

Fig. 7. χ^2 distributions for the n - p elastic scattering data and for the
Monte Carlo (⊓⊓⊓⊓) simulation of the process. The Monte Carlo distri-
bution has been normalized to the same number of events as the
data (⌐‾‾‾¬).

Fig. 8. Probability of multiple neutron counter events versus energy of
the neutron.

Fig. 9. Relative spatial and time distribution of double neutron counter
events. One counter unit is nearest neighbor, two counter units
is next nearest neighbor, etc.

Fig. 10. Neutral cross scattering probability distributions.

Fig. 11. Total probability of neutral cross scattering versus energy,
i.e., ratio of counts in secondary counters to counts in primary
counter.
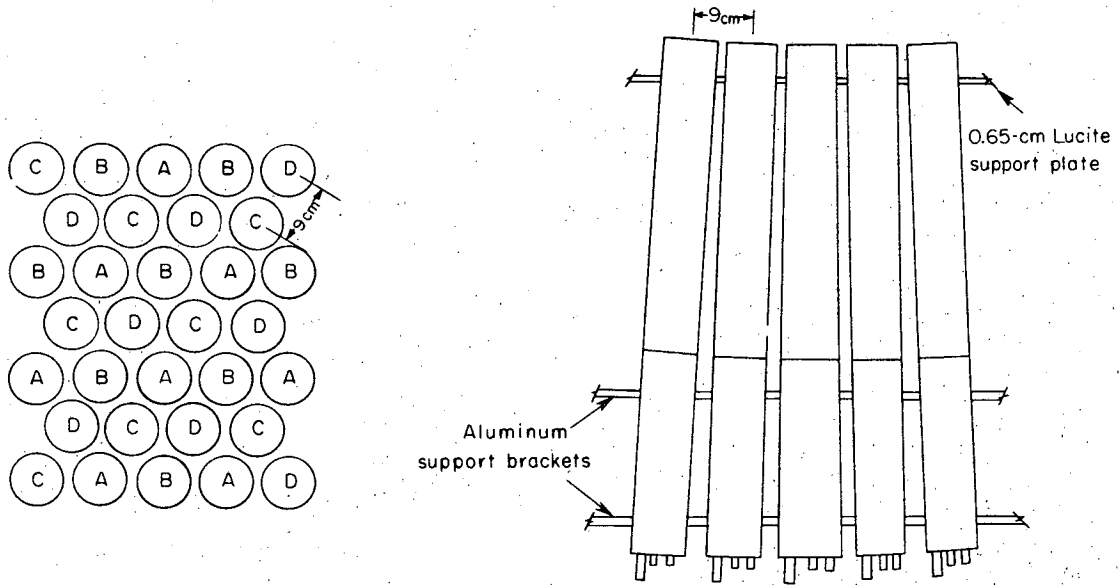
Fig. 1   XBL697-3254
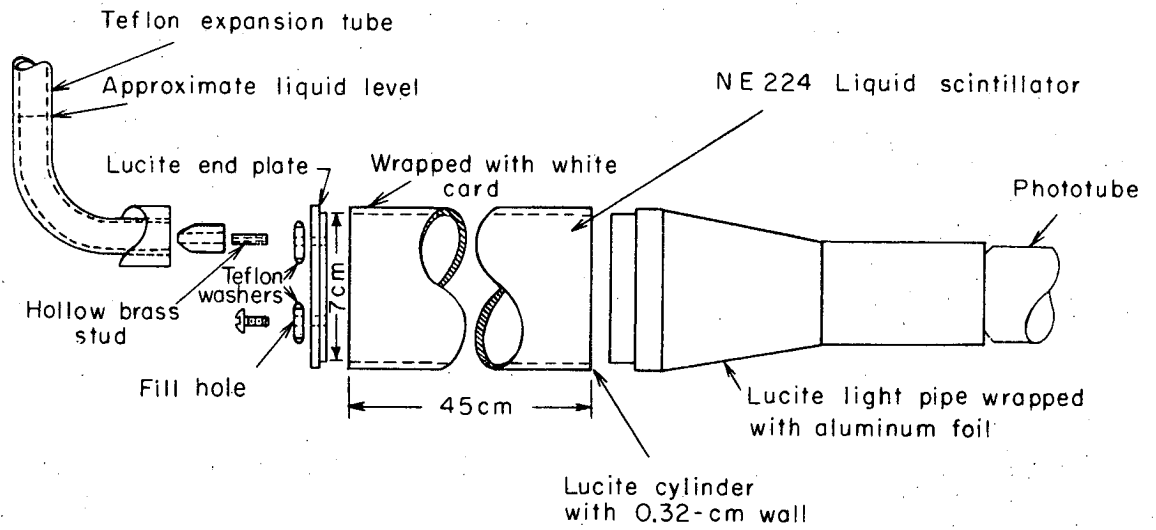
Fig. 2   XBL 697-3256
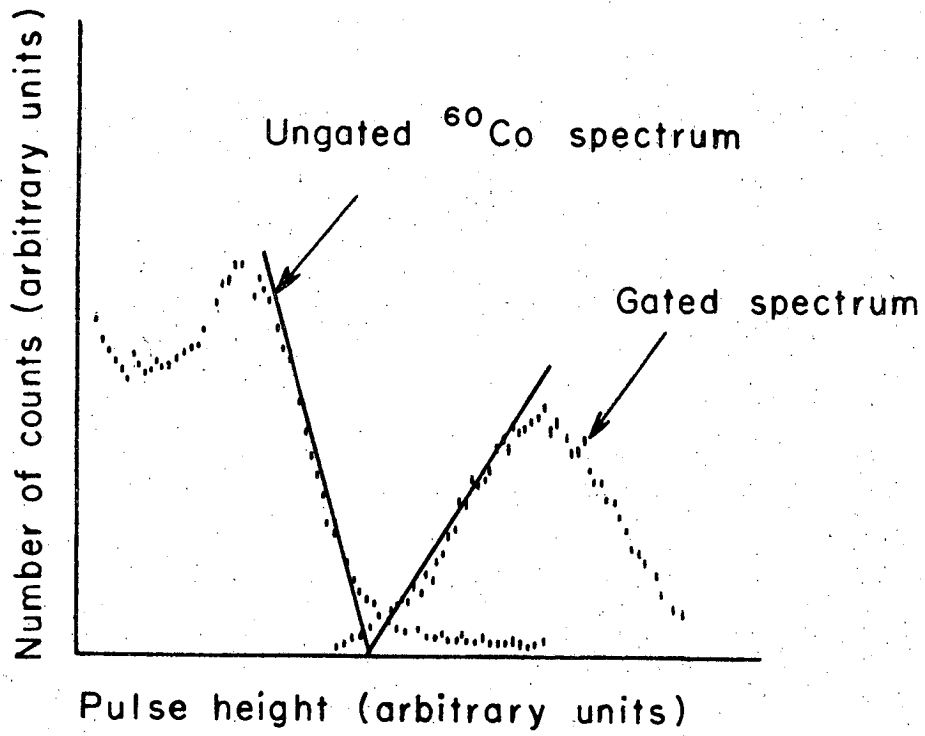
Fig. 3   XBL697- 3249
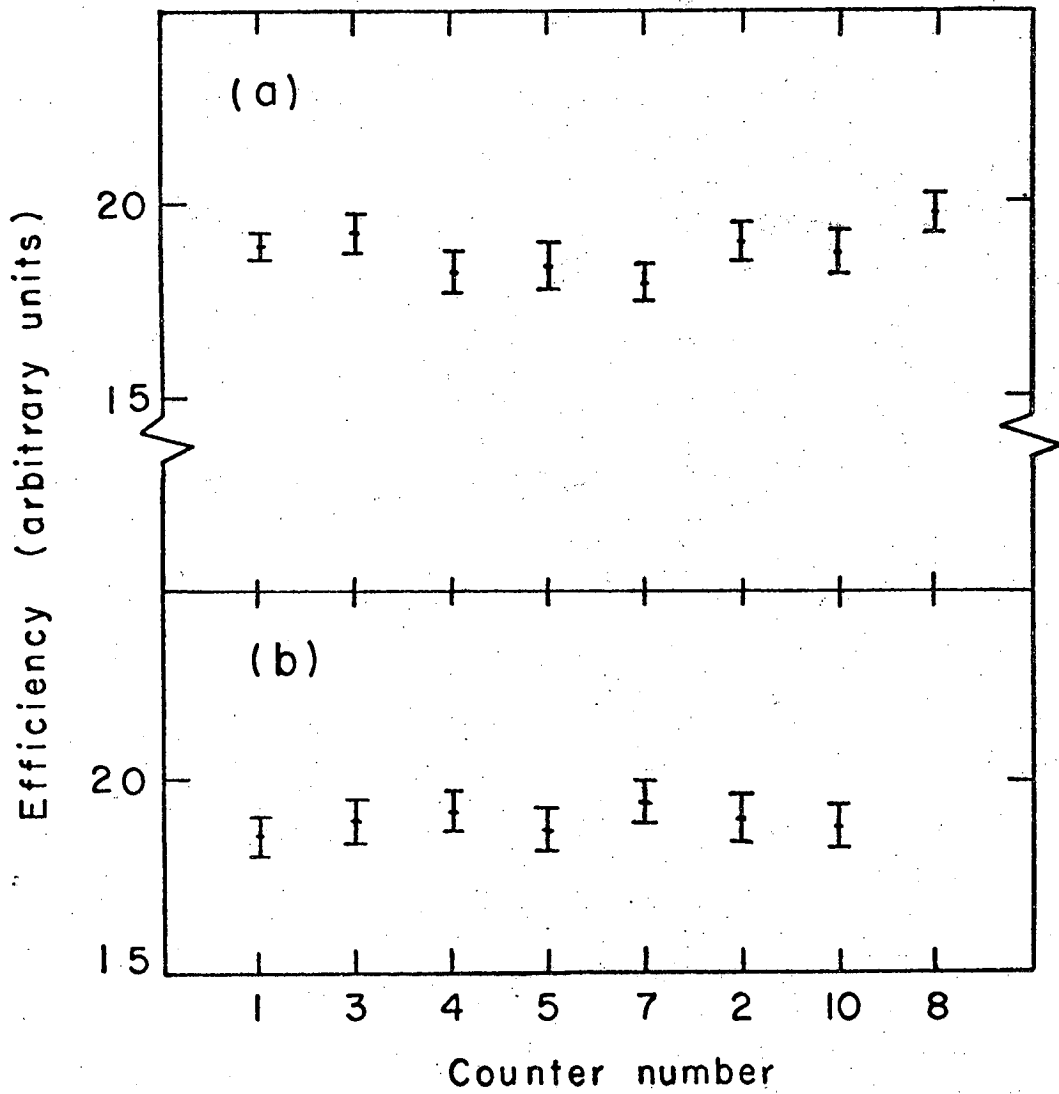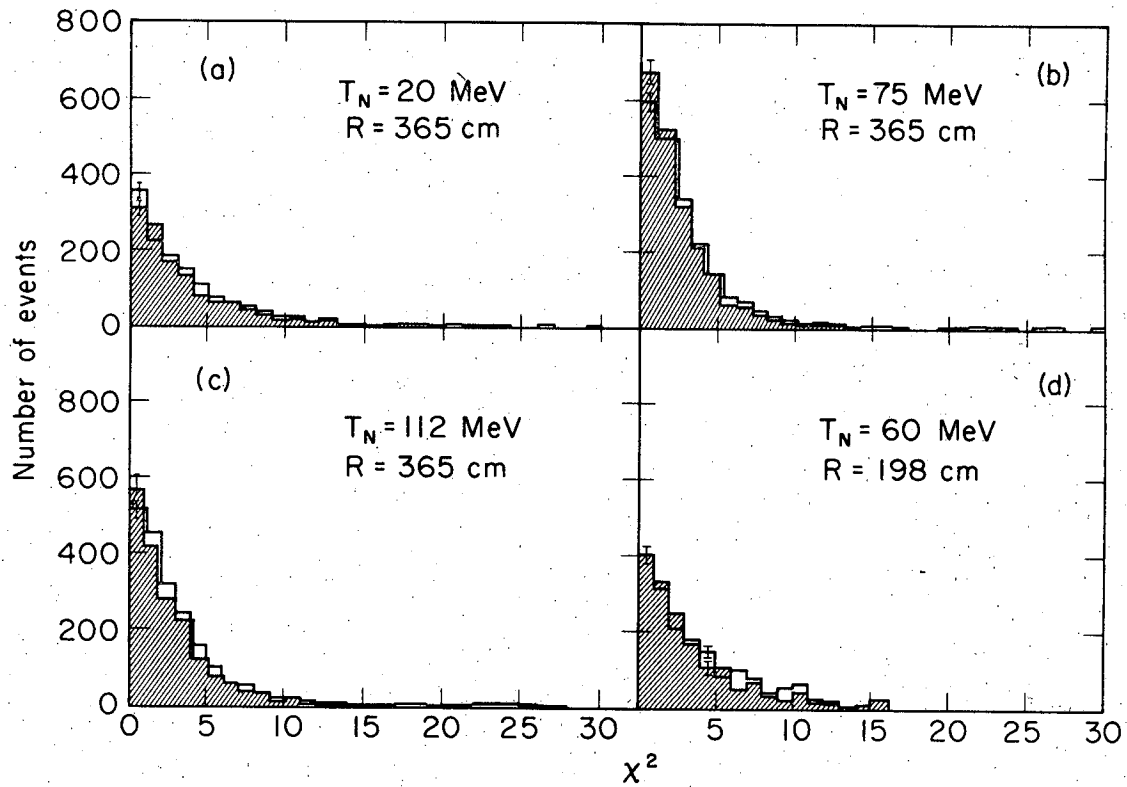
Fig. 4   XBL697-3253
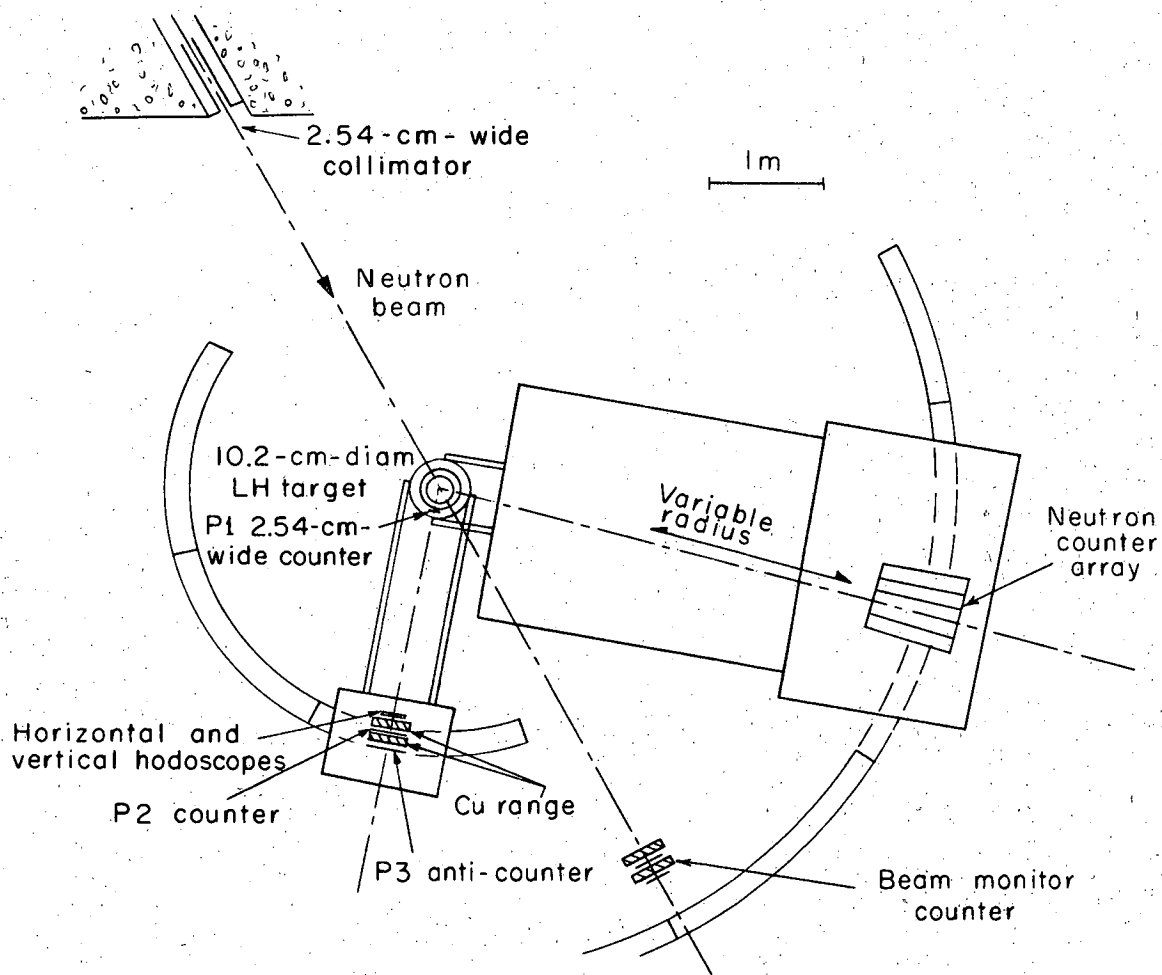
Fig. 5   XBL697-3257
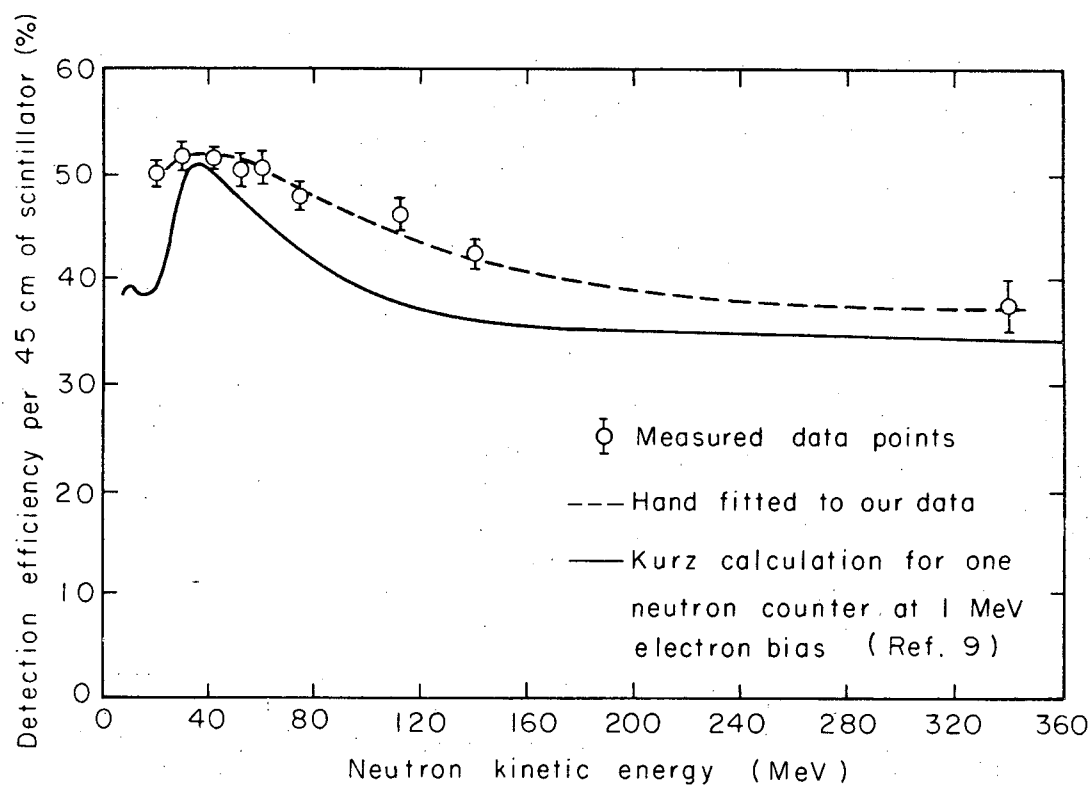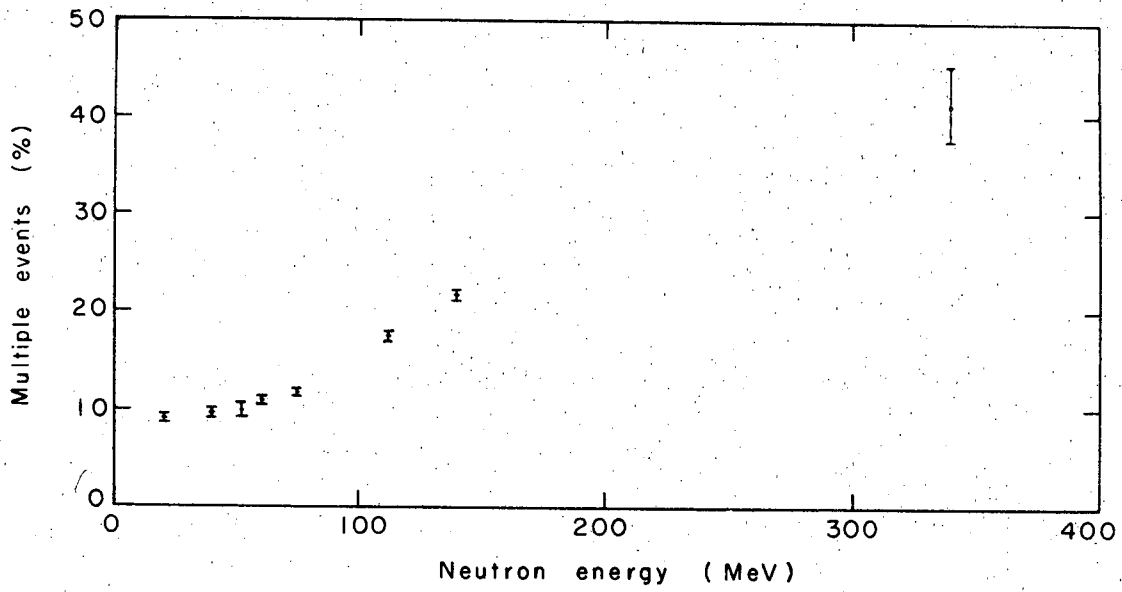
Fig. 6

XBL698-3622

Fig. 7

Fig. 8

XBL 697-3252
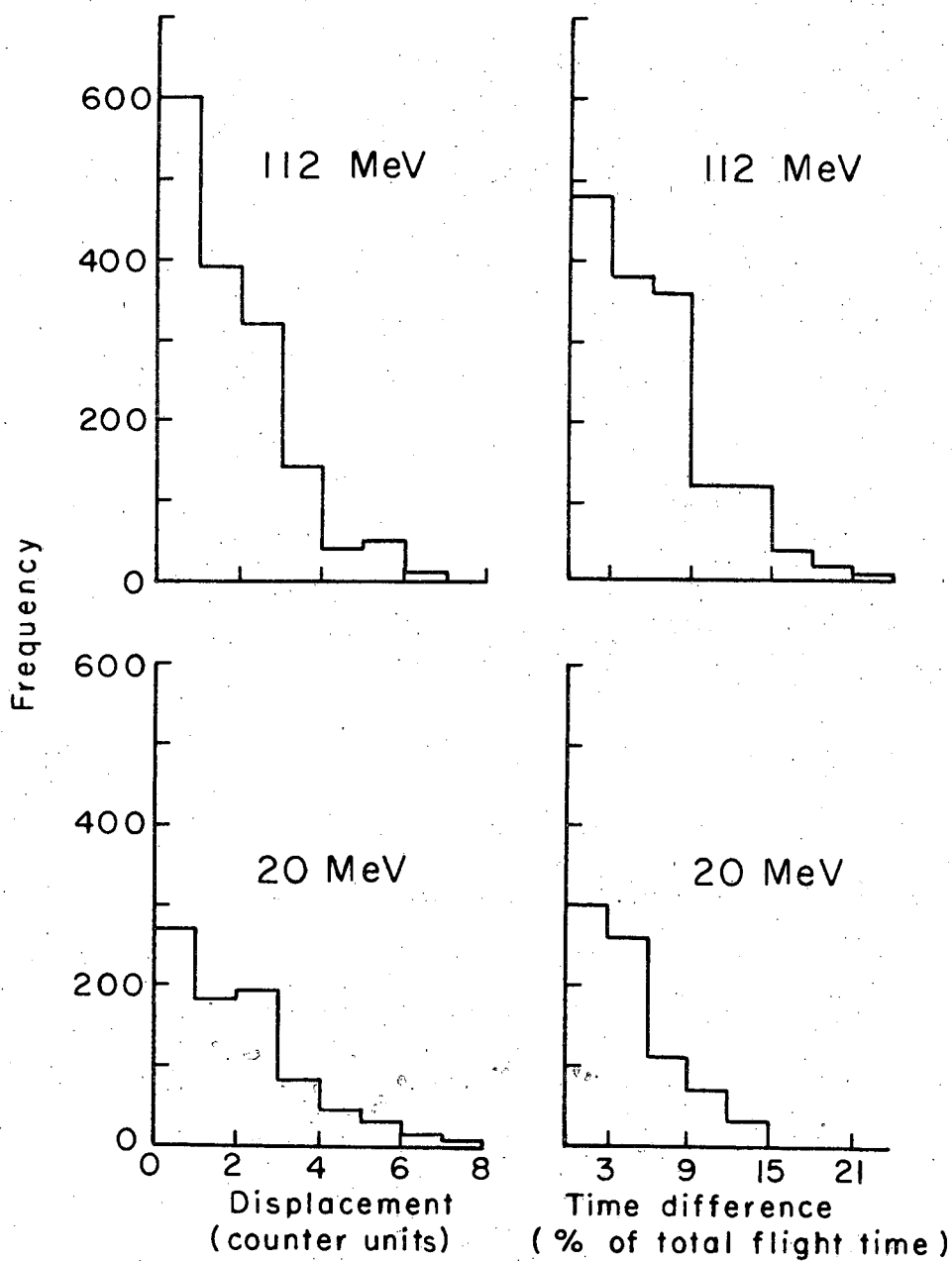
Fig. 9   XBL697-3250
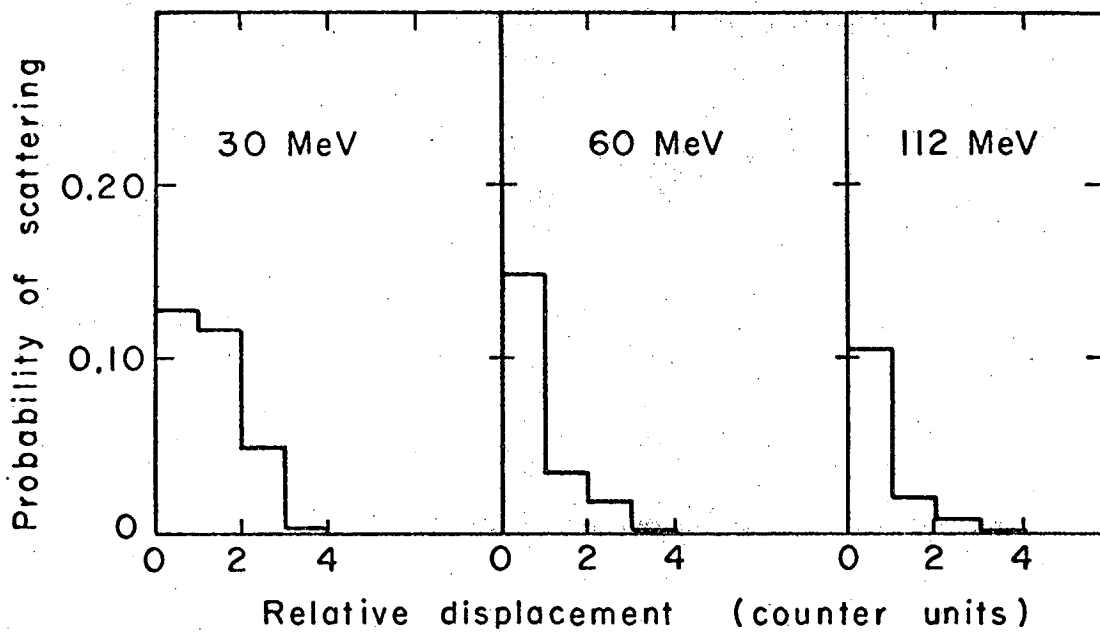
Fig. 10   XBL697-3251
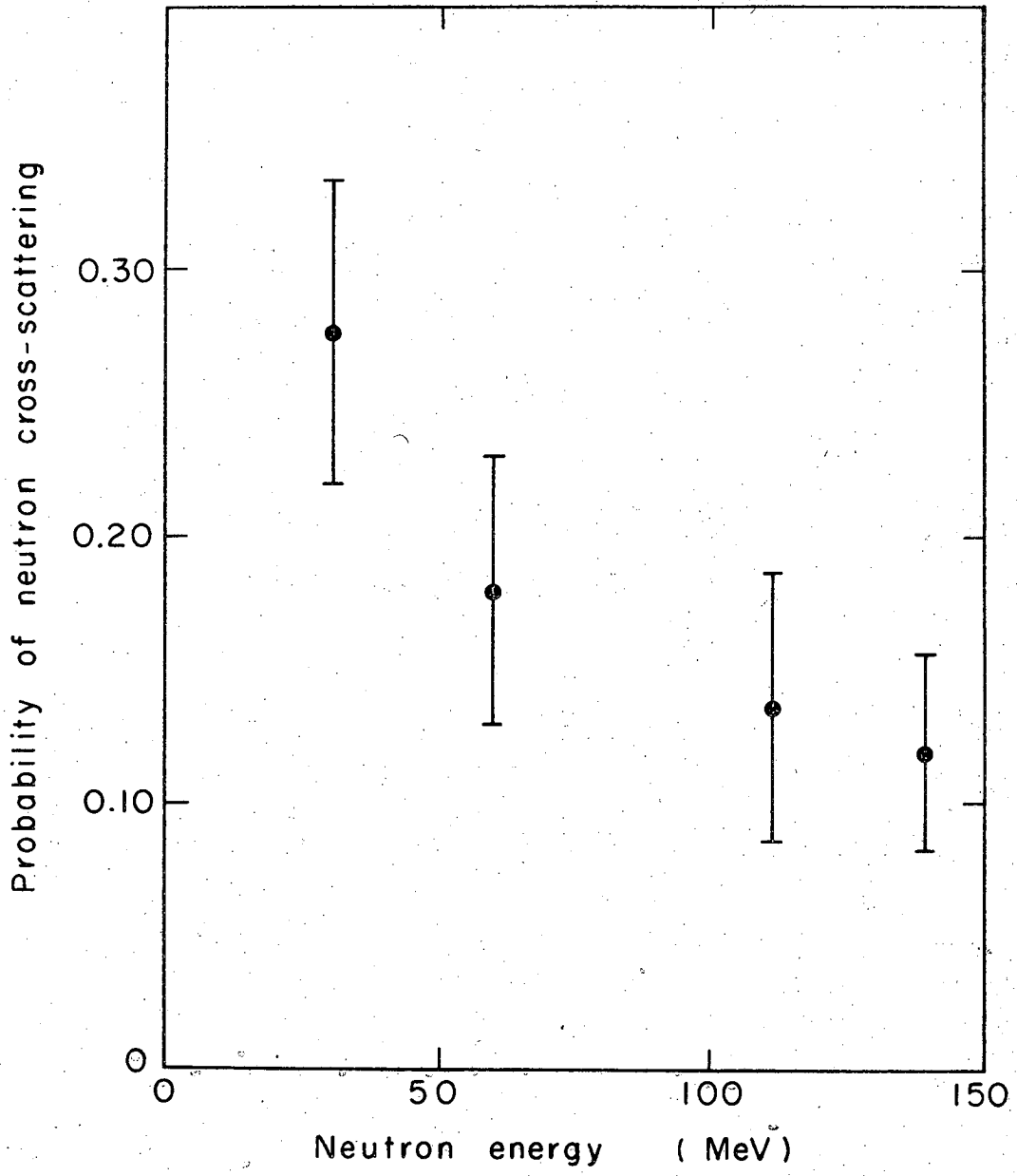
Fig. 11   XBL697-3255